IOP Publishing New J. Phys. 27 (2025) 023011 https://doi.org/10.1088/1367-2630/adac83

New Journal of Physics
The open access journal at the forefront of physics

Deutsche Physikalische Gesellschaft DPG
IOP Institute of Physics

Published in partnership with: Deutsche Physikalische Gesellschaft and the Institute of Physics

OPEN ACCESS

RECEIVED
12 June 2024

REVISED
1 December 2024

ACCEPTED FOR PUBLICATION
21 January 2025

PUBLISHED
7 February 2025

PAPER

Feasibility and parameter optimization of ground-to-satellite uplink continuous-variable quantum key distribution

Jin Cheng, Yujie Chen, Ao Liu, Xin Sun, Junjie Guo, Bohan Yang, Peng Yin, Wenbo Liu, Lanjian Chen* and Chen Dong*

Information and Communication College, National University of Defense Technology, WuHan, People's Republic of China
* Authors to whom any correspondence should be addressed.

E-mail: troy_elephant@163.com and dongchengfkd@163.com

Keywords: continuous-variable quantum key distribution, ground-to-satellite, uplink

Abstract

Driven by the necessitates of wide-area quantum secure communication networks, ground-to-satellite quantum key distribution (QKD) has been highlighted in the field of quantum information. Continuous variable QKD (CV-QKD) shows the advantages of a high secure key rate generation and compatibility in the fiber channel, but the communication range is limited by low attenuation tolerance. In this study, the feasibility of the uplink CV-QKD for Very Low Earth Orbit satellite is studied, and the influence of practical factors such as atmospheric turbulence and beam pointing errors under dynamic time-varying satellite orbital parameters is analyzed to model realistic transmission channels. A parameter optimization scheme for orbital parameters, spot size, receiving telescope aperture, and modulation variance has been proposed to enhance the performance of the actual uplink CV-QKD, providing a reference for parameter selection in CV-QKD experiments.

1. Introduction

Quantum key distribution (QKD) provides secure keys guaranteed by quantum mechanics [1]. At present, the fiber-based QKD protocols are relatively mature [2], and the quantum satellite 'Micius 'verifies the feasibility of satellite-to-ground quantum teleportation, discrete variable QKD (DV-QKD), and entanglement distribution experiments [3], which validated the feasibility of free space DV-QKD, making the wide-area QKD network possible [4].

Compared with the DV-QKD, the CV-QKD has the advantages of higher secure rate and compatibility in optical fiber channels [5], which makes it likely to be generalized to space channel. Although the research work on the feasibility of the CV-QKD in space is in the early stages of theoretical research, it is still necessary to analyze the feasibility of the protocol in the actual environment. Dequal *et al* [6] analyzed the downlink Gaussian modulation CV-QKD in low-orbit satellites under reverse reconciliation. References [7, 8] analyzed the theoretical limit and the practical security rate of coherent state transmission in turbulent channels. In [9], the noiseless attenuation scheme is assumed to analyze the performance of uplink CV-QKD. The previous studies have adopted ideal zenith-crossing circular orbit models with fixed-parameter. This paper delves into the feasibility and parameter optimization of ground-to-satellite uplink CV-QKD. It employs a dynamic operational orbit model that reflects real conditions of satellites by incorporating actual orbit parameters and accounting for the dynamic movements of satellites around the Earth. This model is more significantly affected by turbulence [10].

In this study, the feasibility of Gaussian modulation CV-QKD in uplink is investigated by simulation based on the time-varying orbital motion model. The influence of practical factors such as diffraction, extinction, turbulence, and pointing errors on the uplink channel is analyzed to model realistic transmission channels. A parameter optimization scheme for orbital parameters, spot size, receiving telescope aperture, and modulation variance has been proposed to enhance the performance of the actual uplink CV-QKD, which provides theoretical support for subsequent space channel CV-QKD experiments.

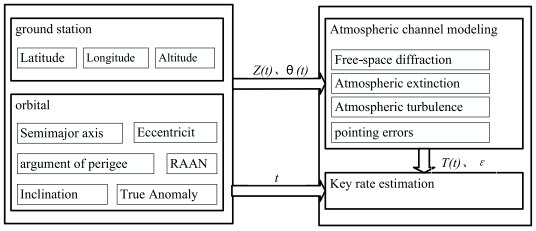

Figure 1. The framework for modeling uplink CV-QKD.

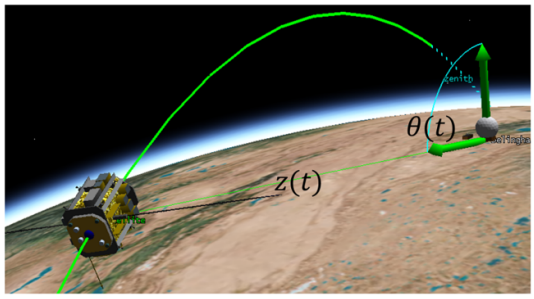

Figure 2. Schematic diagram of CV-QKD communication scheme. A fixed ground station (Alice) and a satellite (Bob) follows a self-defined trajectory.

2. Protocol model

This study constructed a model of the ground-to-satellite uplink CV-QKD, which includes satellite orbit modeling, atmospheric channel modeling, and key rate estimation. The framework for the modeling shown in figure 1 is described as follows.

Step 1. Longitude, latitude, and altitude are utilized to establish the ground station's geographic coordinates. The semimajor axis, eccentricity, argument of perigee, RAAN, inclination, and true anomaly are parameters integral to the construction of the satellite's orbital model. The foundational architecture of the scenarios is demonstrated by the integration of ground stations and the satellite orbit, which provides parameters such as access duration and link geometry information to determine the time t, zenith angle $\theta(t)$ and distance $z(t)$ between the satellite and the ground station.

Step 2. In the atmospheric channel model, the link loss is calculated by analyzing factors such as free-space diffraction, atmospheric extinction, atmospheric turbulence, and pointing errors, all predicated on dynamic parameters.

Step 3. At last, the secret key rate can be estimated to analyze the feasibility of the CV-QKD.

2.1. Communication modeling

In this study, the detection system is situated on the satellite, while the coherent source is positioned at the ground station. The satellite orbits at an altitude h beyond the Kármán line ($h \geq 100$km). The zenith angle $\theta(t)$ and the slant distance $z(t)$ between the satellite and the ground station are time-dependent functions. The geometric relationship is illustrated in figure 2. This research employs the Satellite Toolkit to construct self-defined satellite and ground station models [11].

At the ground station, we have a tracking system in place to follow the satellite's trajectory, a pilot signal generator that transmits reference symbols, and an adaptive optics (AO) system [12–15] which is worked in a pre-compensation regime. The satellite receiver is equipped with a pilot signal generator. The implementation of the transmit AOs requires Bob to send a strong beacon light to Alice before the communication officially begins. Alice then uses the wavefront phase information of the beacon light to pre-correct the wavefront of the quantum signal being sent [16].

The satellite receiver is equipped with a fiber-coupled coherent detector with a free-running local oscillator (local LO).

2.2. Atmospheric channel modeling

During the beam propagation process, various disturbance effects come into play [17], with the severity being intimately linked to the satellite's running time t. In this study, the effects of free-space diffraction,

atmospheric extinction, weak atmospheric turbulence and pointing errors on uplink beam propagation at night are analyzed to calculate the transmission efficiency.

In the context of weak atmospheric turbulence at night, and with the incorporation of an AOs system to correct for turbulence, subsequent simulation analyses will exclude the probability of interruptions caused by fluctuations in the angle of arrival [16].

2.2.1. Free-space diffraction

We postulate that the ground station emits a collimated Gaussian beam characterized by a carrier wavelength of $\lambda = 800\text{nm}$. The beam's initial spot size is denoted as w_0, and the radius of curvature [18] is $R_0 = \infty$. When the beam has propagated a distance $z(t)$, the spot size at the receiver can be expressed by the Gaussian beam propagation equation [7]:

$$w_d(t) = w_0\sqrt{\left(1-\frac{z(t)}{R_0}\right)^2+\left(\frac{z(t)}{z_R}\right)^2} \tag{1}$$

where $z_R = \pi w_0^2\lambda^{-1}$ is the Rayleigh range. Since the radius of the receiver telescope on the satellite is a_R, the diffraction-induced transmission efficiency [7] can be given by:

$$\eta_d(t) = 1-\mathrm{e}^{-\frac{2a_R^2}{w_d^2(t)}}. \tag{2}$$

2.2.2. Atmospheric extinction

Considering the zenith angle $\theta(t)$ between the satellite and the ground station, the atmospheric transmission efficiency [6] can be approximated as:

$$\eta_{\text{atm}}(t) \approx \eta_{\text{atm}}^{\text{zen}\,\sec(\theta(t))}. \tag{3}$$

Where $\eta_{\text{atm}}^{\text{zen}} = \mathrm{e}^{-\int_0^h \mathrm{d}h'\alpha(h')} \geqslant \mathrm{e}^{-\alpha_0\tilde{h}} \approx 0.967$ [8] is the transmission efficiency at the zenith. $\alpha(h) = \alpha_0\mathrm{e}^{-h/\tilde{h}}$ is the is the extinction factor, where $\tilde{h}$= 6600 m. $\alpha_0 = 5\times10^{-6}\ \text{m}^{-1}$ at $\lambda = 800\text{nm}$.

2.2.3. Atmospheric turbulence

Atmospheric turbulence can induce beam deflection and broadening, which in turn leads to signal fading. Specifically, in the uplink, the turbulence causes the spot size on the receiver to increase according to the following relationship:

$$w_{\text{st}}^2(t) \approx w_d^2(t) + z^2\Delta(\theta(t)) \tag{4}$$

where $\Delta(\theta(t)) = \frac{26.28I_\infty\sec\theta^{6/5}}{\lambda^{2/5}} - \frac{7.71I_\infty\sec\theta}{w_0^{1/3}}$. In these formulas, I_∞ takes different values depending on the atmospheric model (H-V model). This manuscript takes $I_\infty \approx 2.2354\times10^{-12}\ \text{m}^{1/3}$ at night, and $I_\infty \approx 23.2854\times10^{-12}\ \text{m}^{1/3}$ at day [8].

Therefore, diffraction-induced transmission efficiency is replaced by turbulence-induced transmission efficiency [7]:

$$\eta_{st}(t) = 1-\mathrm{e}^{-\frac{2a_R^2}{w_{\text{st}}^2(t)}}. \tag{5}$$

Considering the free-space diffraction, atmospheric extinction, atmospheric turbulence and inevitable fixed loss [6] η_{ATT} (assumes $\eta_{\text{ATT}} = 3.8$ dB, including 3 dB of losses for fiber coupling and an additional 0.8 dB for taking into account the fact that we are only considering the main peak of the Airy diffraction pattern), the total transmission efficiency can be given by:

$$\eta_{\text{tot}}(t) = \eta_{\text{ATT}}\eta_{\text{atm}}(t)\,\eta_{\text{st}}(t)\ . \tag{6}$$

It is worth noting that equation (6) represents the transmission efficiency without considering the beam deflection. When beam deflection is taken into account, equation (6) denotes the maximum achievable transmission efficiency. The beam deflection is characterized by the wandering of the beam's centroid according to a Gaussian distribution with variance given by [8]:

$$\sigma_{\text{TB}}^2(t) \approx \frac{7.71I_\infty}{w_0^{\frac{1}{3}}}z^2\sec\theta(t). \tag{7}$$

2.2.4. Pointing errors

Pointing errors can also lead to beam deflect. We assumed $\theta_p = 10^{-6}$rad, which leads to another random deflection, whose variance [8] can be approximated as:

$$\sigma_P^2(t) \approx \left(\theta_p z(t)\right)^2. \tag{8}$$

Therefore, the total variance of the random deflection of the beam's centroid can be given by:

$$\sigma^2(t) = \sigma_P^2(t) + \sigma_{\mathrm{TB}}^2(t). \tag{9}$$

The deflection of the beam's centroid will cause the instantaneous transmission efficiency to be $T(t) \leqslant \eta_{\mathrm{tot}}(t)$.

In case of weak turbulence and considering a wavelength of 800 nm, the probability distribution of the deflection distance follows the Wei-bull distribution [19], and $T(t)$ obeys the probability distribution $P_\sigma(T)$ [8]:

$$P_\sigma(T) = \frac{r_0^2}{\gamma\sigma^2 T(t)}\left(\ln\frac{\eta_{\mathrm{tot}}(t)}{T(t)}\right)^{\frac{2}{\gamma}-1}\exp\left[-\frac{r_0^2}{2\sigma^2}\left(\ln\frac{\eta_{\mathrm{tot}}(t)}{T(t)}\right)^{\frac{2}{\gamma}}\right] \tag{10}$$

where

$$\gamma(t) = \frac{4\frac{2a_R^2}{w_{\mathrm{st}}^2(t)}f_0\left(\frac{2a_R^2}{w_{\mathrm{st}}^2(t)}\right)f_1\left(\frac{2a_R^2}{w_{\mathrm{st}}^2(t)}\right)}{\ln\left[2\eta_{\mathrm{st}}(t)f_0\left(\frac{2a_R^2}{w_{\mathrm{st}}^2(t)}\right)\right]} \tag{11}$$

$$r_0(t) = \frac{a_R}{\ln\left[2\eta_{\mathrm{st}}(t)f_0\left(\frac{2a_R^2}{w_{\mathrm{st}}^2(t)}\right)\right]^{1/\gamma(t)}} \tag{12}$$

$$f_0(x) = \left[1-\exp(-2x)I_0(2x)\right]^{-1} \tag{13}$$

$$f_1(x) = \exp(-2x)I_1(2x) \tag{14}$$

I_n is the first kind of modified Bessel function with order $n = 0, 1$.

2.3. Secure key rate estimation

According to the previous analysis of the atmospheric channel, the actual instantaneous transmission efficiency $T(t)$ is a random variable. We propose employing a beacon signal to estimate the instantaneous channel transmission efficiency. The fading channel can be modeled as an equivalent non-fading channel, characterized by a fixed effective transmittance $T_{\mathrm{e}}(t)$.

Given the relatively small additional noise caused by phase recuperation[6, 8], this paper treats the excess noise as a single parameter, denoted by ε, which represents the excess noise at Alice's side.

For the excess noise ε, $\varepsilon_{\mathrm{e}}(t)$ is used as the equivalent excess noise[16, 20].

$$\begin{cases} T_{\mathrm{e}}(t) = E\left[\sqrt{T(t)}\right]^2 \\ \varepsilon_{\mathrm{e}}(t) = \frac{E[T(t)]}{E\left[\sqrt{T(t)}\right]^2}\varepsilon + \frac{\mathrm{Var}\left(\sqrt{T(t)}\right)(V-1)}{E\left[\sqrt{T(t)}\right]^2} \end{cases}. \tag{15}$$

Where $E\left[\sqrt{T(t)}\right] = \int_0^{\sqrt{\eta_{\mathrm{tot}}(t)}}\sqrt{T(t)}P\left(\sqrt{T(t)}\right)\mathrm{d}\sqrt{T(t)}$ is the expectation of $\sqrt{T(t)}$, and $\mathrm{Var}\left(\sqrt{T(t)}\right) = E[T(t)] - E\left[\sqrt{T(t)}\right]^2$ describes the strength of the channel fluctuations.

In the case of reverse reconciliation, the asymptotic value of the secret key rate can be written as [20, 21]:

$$R = \beta I_{AB} - \chi_{BE}. \tag{16}$$

The channel-added noise referred to the channel input, is defined as $\chi_{\mathrm{line}} = \frac{1}{T_{\mathrm{e}}} - 1 + \varepsilon_{\mathrm{e}}$. An actual detector has the detection efficiency η and the electronic noise vel. The detection-added noise referred to Bob's input is defined as $\chi_{\mathrm{hom}} = [(1-\eta) + \mathrm{vel}]/\eta$ and $\chi_{\mathrm{het}} = [1 + (1-\eta) + 2\mathrm{vel}]/\eta$ for homodyne and heterodyne detection, respectively. So, the total noise referred to the channel input can then be expressed as $\chi_{\mathrm{tot}} = \chi_{\mathrm{line}} + \chi_{\mathrm{h}}/T_{\mathrm{e}}$

Alice prepares the coherent states according to a Gaussian distribution with variance $V_A N_0$, where N_0 is the shot noise variance. We can define $V = V_A + 1$. The mutual information of Alice and Bob for homodyne and heterodyne detection can be written as:

$$I_{AB}^{\text{hom}} = \frac{1}{2}\log_2 \frac{V + \chi_{\text{tot}}}{1 + \chi_{\text{tot}}} \tag{17}$$

$$I_{AB}^{\text{het}} = \log_2 \frac{V + \chi_{\text{tot}}}{1 + \chi_{\text{tot}}} . \tag{18}$$

The maximum amount of information that the Eve can potentially extract from Bob is bounded by the Holevo quantit

$$\chi_{BE} = S(\rho_{AB1}) - S(\rho_{AFG}^{mB}) = \sum_{i=1}^{2} G\left(\frac{\lambda_i - 1}{2}\right) - \sum_{i=3}^{5} G\left(\frac{\lambda_i - 1}{2}\right) \tag{19}$$

where $G(x) = (x+1)\log_2(x+1) - x\log_2 x$, and $\lambda_{1,2}$ are the symplectic eigenvalues of the covariance matrix γ_{AB1} characterizing the state ρ_{AB1}, and $\lambda_{3,4,5}$ are the symplectic eigenvalues of the covariance matrix γ_{AFG}^{mB} characterizing the state ρ_{AFG}^{mB} [22].

The covariance matrix γ_{AB1} is:

$$\gamma_{AB1} = \begin{bmatrix} V \cdot I & \sqrt{T_e(V^2-1)} \cdot \sigma_z \\ \sqrt{T_e(V^2-1)} \cdot \sigma_z & T_e(V + \chi_{\text{line}}) \cdot I \end{bmatrix}. \tag{20}$$

When we consider the uncertainty of the parameter estimation due to the limited statistics, the Finite-size value of the secret key rate can be written as [23]:

$$R_{\text{finite}} = \frac{n}{N}\left[\beta I_{AB} - \mathcal{X}_{\epsilon_{\text{PE}}} - \Delta(n)\right]. \tag{21}$$

Given the clock rate C = 1 GHz, there are N = C symbols exchanged in 1 s. Out of these N symbols, only n = N − m symbols are used for establishing the key, with m = 0.1 N symbols dedicated to parameter estimation.

What needs to be clarified is that, with a sampling rate higher than the atmospheric coherence time (typically around 1 kHz), the ground station transmits pilot signals and beacon lights, and the detection of the beacon signal's intensity at the satellite receiver can achieve parameter estimation of the transmission efficiency for each point on the orbit during the fading process [6].

$\mathcal{X}_{\epsilon_{\text{PE}}}$ represents the information that Eve manages to intercept when Alice's estimation of Bob's channel parameters has an error probability of ϵ_{PE}. This effect is accounted by considering a lower bound on transmission coefficient $T_{\min}$ to replace transmission efficiency $T(t)$ and an upper bound of excess noise $E(\varepsilon_{\max}(t))$ to replace the excess noise ε [16],

$$\begin{cases} T_{\min}(t) = (\sqcup_{\min}(t))^2 \\ \varepsilon_{\max}(t) = \frac{\sigma_{\max}^2(t) - 1}{T_{\min}(t)} \end{cases} \tag{22}$$

where $z_{\epsilon_{\text{PE}}/2}$ is a parameter related to the estimated probability of failure ϵ_{PE}. (Here we consider ϵ_{PE}=10^{-10}, which gives $z_{\epsilon_{\text{PE}}/2} = 6.5$)

$$\begin{cases} \sqcup_{\min}(t) \approx \sqrt{T(t)} - z_{\epsilon_{\text{PE}}/2}\sqrt{\frac{1+T(t)\varepsilon}{mV_A}} \\ \sigma_{\max}^2(t) \approx 1 + T(t)\varepsilon + z_{\epsilon_{\text{PE}}/2}\frac{(1+T(t)\varepsilon)\sqrt{2}}{\sqrt{m}} \end{cases} . \tag{23}$$

The parameter $\Delta(n)$ is related to the security of the privacy amplification:

$$\Delta(n) \equiv (2\dim\mathcal{H}_x + 3)\sqrt{\frac{\log_2(2/\epsilon)}{n}} + \frac{2}{n}\log_2(1/\epsilon_{\text{PA}}) \tag{24}$$

where $\mathcal{H}_x$ is the Hilbert space corresponding to the variable x used in the raw key, ϵ is a smoothing parameter, and ϵ_{PA} is the failure probability of the privacy amplification procedure. (Here we consider $\epsilon = 10^{-10}$, $\epsilon_{\text{PA}} = 10^{-10}$, and $\dim\mathcal{H}_x = 2$.)

The total secure key K generated in the access duration [t_start, t_end] can be calculated to be [24]:

$$K = \int_{t\_\text{start}}^{t\_\text{end}} R_{\text{finite}}(t)\, C\mathrm{d}t. \tag{25}$$

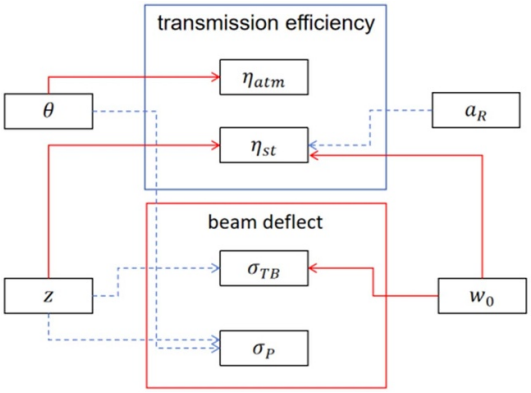

Figure 3. Parameter relationship diagram.

Table 1. Main simulation parameters used in our mode.

Parameter	Symbol	Value
Pointing errors	θ_p	1 μ rad
Extinction (at 0 rad)	$\eta_{\text{atm}}^{\text{zen}}$	0.967
Electronic noise	*vel*	0.1 S.N.U.(shot noise unit)
Detector efficiency	η	0.4
Excess noise	ε	0.01 S.N.U.
Rec. efficiency	β	0.95
Fixed attenuation	η_{ATT}	0.4

3. Simulation results and parameter analysis

The feasibility of uplink CV-QKD, employing reverse reconciliation and heterodyne detection, is assessed within the aforementioned framework. Atmospheric turbulence exerts a relatively more pronounced influence on the uplink, with the induced beam broadening and deflection being correlated to a range of parameters, including propagation distance, zenith angle, initial spot size, and the aperture of the receiving telescope. As depicted in figure 3, the blue dashed line signifies a positive correlation between the two connected variables, while the red solid line denotes a negative correlation.

The main simulation parameters used in model are shown in table 1.

Utilizing real-world parameters as input, our proposed framework serves as a method for conducting a feasibility assessment of space-based CV-QKD within a specific scenario. In this study, we reference the Weber telescope, the largest space optical telescope with a diameter of 6.5 m [25], to limit the parameter boundaries for the receiving telescope aperture and the initial spot size, which are set at 3 m [26, 27]. In this section, we initially conduct a comprehensive exploration of the entire parameter space to find the specific conditions under which feasibility may be achieved. An uplink from the Nagari station to the Micius satellite is modeled to conduct a preliminary feasibility assessment. We conduct an exploration within the parameter space that is compatible with the requirements of the space industry. At the nearest point between the 'Micius 'and the ground station, (the distance is around 501 km and the satellite is at an zenith angle of 14.1°[11]), The variation of link loss is presented in figure 4. The maximum tolerable loss of CV-QKD is presented in figure 5.

As can be seen from figure 5, the secret key cannot be generated when $w_0 \leq 1\,\text{m}$. When $w_0 = 2\,\text{m}$, the maximum tolerable attenuation is approching 10 dB. As illustrated in figure 4, to maintain the link loss beneath 10 dB, a telescope radius a_R of approximately 2.4 m is necessary. An increased telescope radius can substantially decrease the link loss; however, the size of telescopes that can be feasibly mounted on satellites is constrained by cost and complexity, as larger ones are both more expensive and complicated to implement. In the actual application, a trade-off is inevitable between the secret key rate and the associated costs. The selection of values such as $w_0 = 2\,\text{m}$ and $a_R = 2.4\,\text{m}$ is impractical, given the considerable financial outlay.

Consequently, the implementation of uplink QKD at the orbit of the 'Micius' satellite presents an exceedingly challenge at present. Subsequently, we intend to conduct a parameter analysis at lower orbits to find more viable parameter configurations.

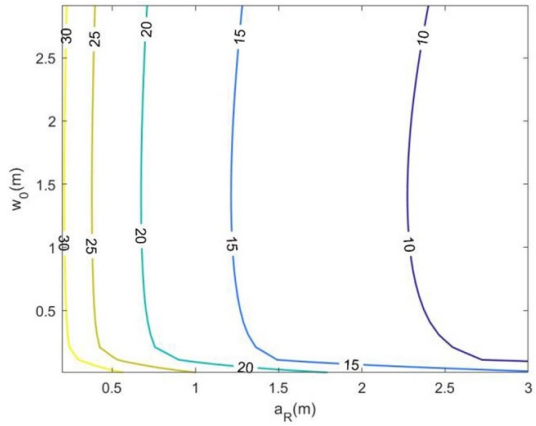

Figure 4. Different factors induced link loss (in dB). $z = 501\,\text{km}$, $\theta = 14.1°$.

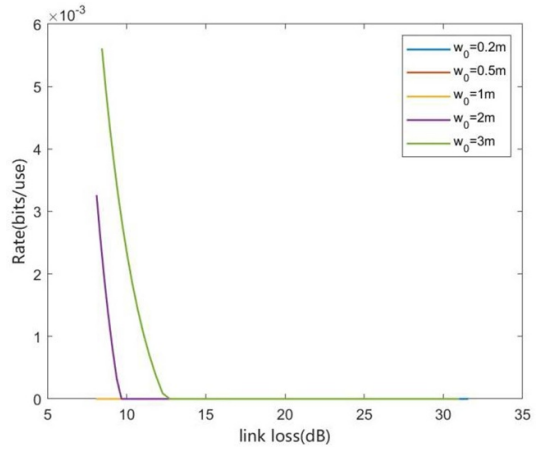

Figure 5. The tolerable loss of CV-QKD. $z = 501\,\text{km}$, $\theta = 14.1°$, V = 2 S.N.U.

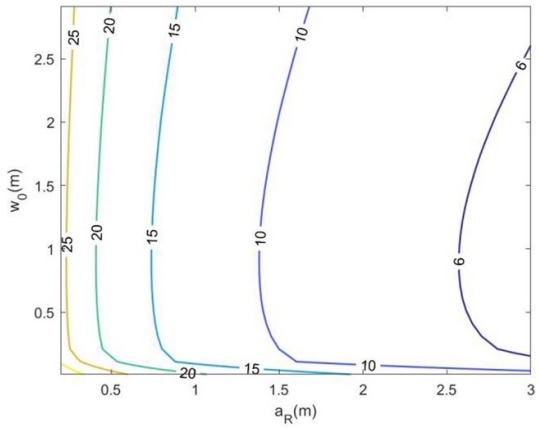

Figure 6. Different factors induced link loss (in dB). $z = 300\,\text{km}$, $\theta = 0°$.

Figures 6 and 7 depict the link loss and the tolerable threshold of link loss for CV-QKD at the zenith of a 300 km orbit, impacted by various parameters. At this juncture, it is evident that w_0 can take on more practical values with $w_0 \leqslant 1$ m, while the telescope aperture a_R still necessitates a significant size to effectively facilitate QKD. Therefore, in the subsequent analysis, we will consider orbital altitudes within 300 km.

Under a certain satellite-based scene model ($h \leqslant 300$ km), the influence of three parameters of receiving aperture, beam spot size and modulation variance on the secret key rate is analyzed to explore the parameter

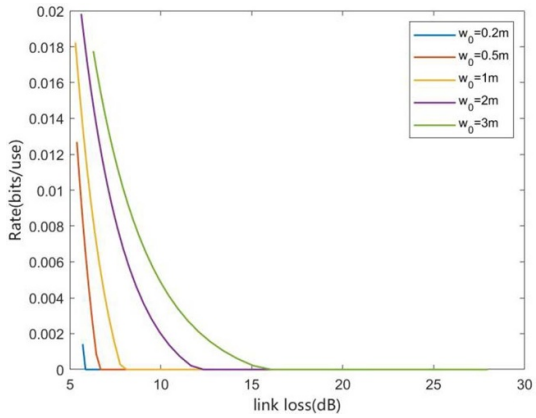

Figure 7. The tolerable loss of CV-QKD, $z = 300$ km, $\theta = 0°$, V = 2 S.N.U.

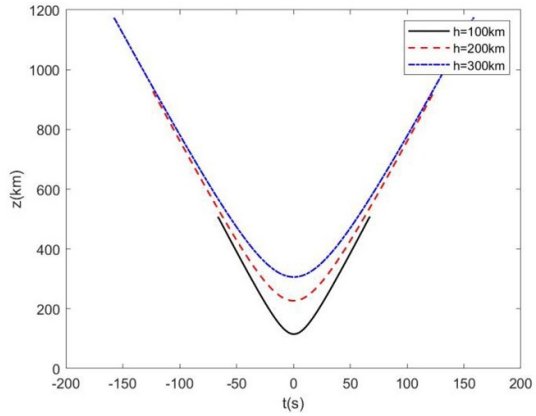

Figure 8. Distance between the satellite and the Delingha station. The lowest distances are approximately 100 km, 200 km and 300 km, respectively.

optimization. It should be pointed out that sats in very low Earth orbits (VLEOs) face a complex dynamic environment and atmospheric resistance, requiring sustained orbital adjustments to mitigate such impacts.

Since most low-orbit satellites have very small ellipticities, mostly in circular or near-circular orbits, this article models dynamic circular orbits with RAAN of $-17°$, an inclination of 55°, and different orbital altitude h of 100 km, 200 km and 300 km. The direct distance $z(t)$ and the change of the zenith angle $\theta(t)$ between the satellite and the Delingha station are shown in figures 8 and 9. It should be noted that the satellite orbit is not the zenith-crossing orbit, so the real-time distance $z(t)$ between the satellite and the ground station is greater than the orbital height h. The interval is 1 s.

What needs to be pointed out is: due to the favorable assumptions regarding telescope dimensions and orbital parameters that ensure a high transmission rate, we can rely on 10^8 symbols to achieve a estimation of parameters and the generation of a finite-length secret key rate.

Figures 10 and 11 shows the influence of the aperture size of the receiving telescope on the secret key rate. Figure 10 shows the real-time secure key rate of h = 100 km under different receiving telescope values. It is obvious that the secret key rate and the generation time of the secret key rate both increase with the increasing telescope aperture size. The comparison of the secure key obtained by equation (20) under different receiving telescope values is shown in figure 11.

From figure 11, it is observed that for the utilization of a more practical telescope aperture, with a radius less than 1 m, key rate generation becomes feasible exclusively at an orbital altitude of 100 km. To continue analyzing the impact of other parameters on the key rate at different orbital heights, this paper employs a receiving telescope radius (a_R) of 2.4 m in subsequent simulations, a value that enables all three orbits to generate non-zero key rates. To further analyze the influence of various parameters on the key rate across different orbital altitudes, this paper adopts a receiving telescope radius (a_R) of 2.4 m for subsequent

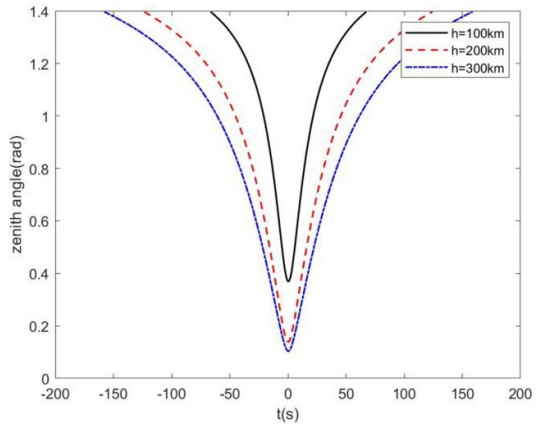

Figure 9. Zenith angle between the satellites and the Delingha station. The lowest zenith angles are more than zero.

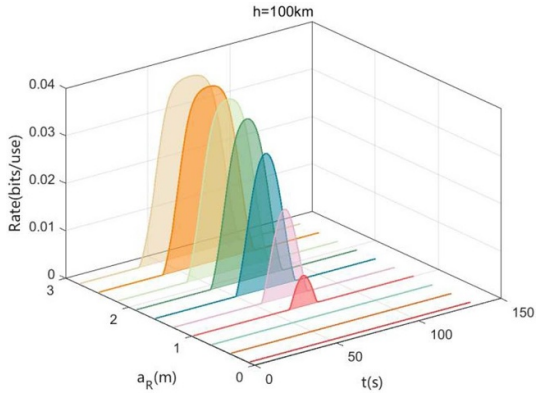

Figure 10. The real-time secure key rate under different a_R, where $h = 100$ km, $w_0 = 0.6$ m, and $V = 2$ S.N.U.

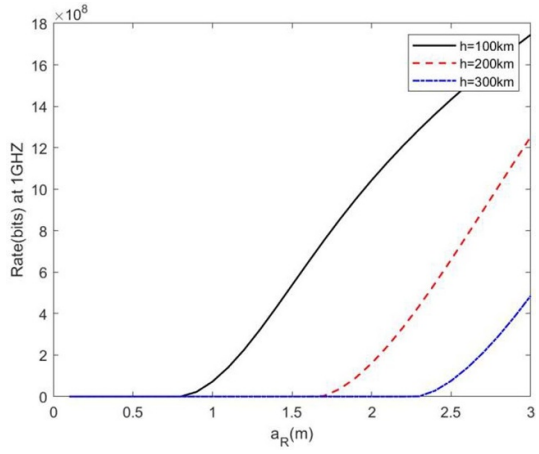

Figure 11. The comparison of the secure key under different a_R, where $V = 2$ S.N.U, and $w_0 = 0.6$ m.

simulations. This radius is selected as it facilitates the generation of non-zero key rates for all three considered orbits. However, it must be additionally emphasized that this selected value remains somewhat optimistic and may not fully account for all practical constraints.

Figures 12 and 13 shows the influence of the initial spot size on the secret key rate ($a_R = 2.4$m). Figure 12 present the real-time secure key rate of $h = 100$ km with different initial spot sizes. It can be seen that there exists an optimal initial spot size to obtain the maximum secret key rate. For the uplink, the transmitter is at

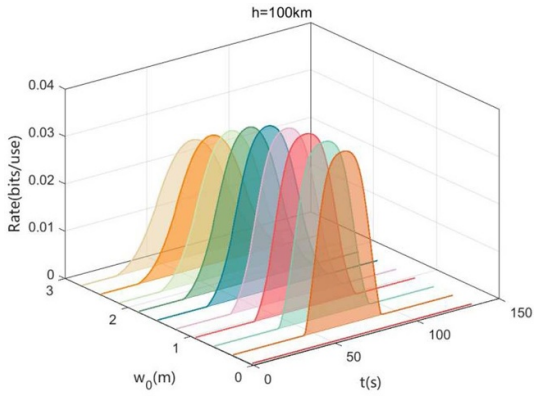

Figure 12. The real-time secret key rate with different w_0, where $h = 100$ km, $a_R = 2.4$m, and $V = 2$ S.N.U.

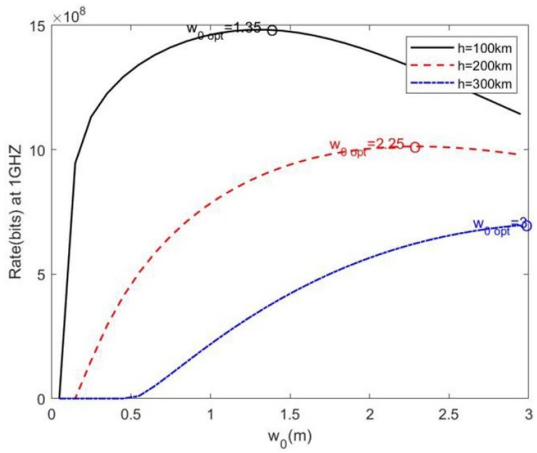

Figure 13. The secure key with different w_0, where $a_R = 2.4$ m, and $V = 2$ S.N.U.

the ground station, and the initial spot size can be adjusted according to the specific satellite orbit to obtain the maximum secret key rate. The secure key generated with different initial spot sizes is shown in figure 13. For the altitude of 100 km, 200 km and 300 km, the optimal w_0 can be set as 1.35 m, 2.25 m, 3 m to obtain the maximized secure key. It is evident that the optimal initial spot size will increase with orbital altitude.

Figure 14 shows the influence of the aperture of the receiving telescope and the initial spot size on the secret key, and (a) (b) (c) are the contour maps of secure key of different altitudes. The blue-green area in the image is a non-zero secret key area, which is concentrated in the upper part of the image. It can be seen that increasing the aperture of the receiving telescope a_R has a significant effect on improving the secret key rate. By comparing (a) (b) (c), it is visible that the non-zero secret key region shrinks with increasing satellite orbit height. Increasing the aperture of the receiving telescope has a significant effect on improving the secret key rate. The change trend of contour line with w_0-axis is gentler than that with a_R-axis, which means w_0 has a relatively small impact on the key rate. Therefore, the importance of the choice of a_R on the secure key is highlighted.

Figures 15 and 16 shows the impact of modulation variance on secret key rate. The real-time secure key rate of $h = 100$ km under various modulation variations is illustrated in figure 15. It can be observed that the modulation variance has an effect on the amount of the secret key rate, but has no effect on the duration of the secret key generation. The secret key rate initially increases with the increase of the modulation variance. After the optimal modulation scheme is obtained, the secret key rate decreases with the increase of the modulation variance. Figure 16 reveals the secure key generated under various modulation variances. By comparing the secure key curves at different orbital altitudes, it can be seen that the higher the orbital height,

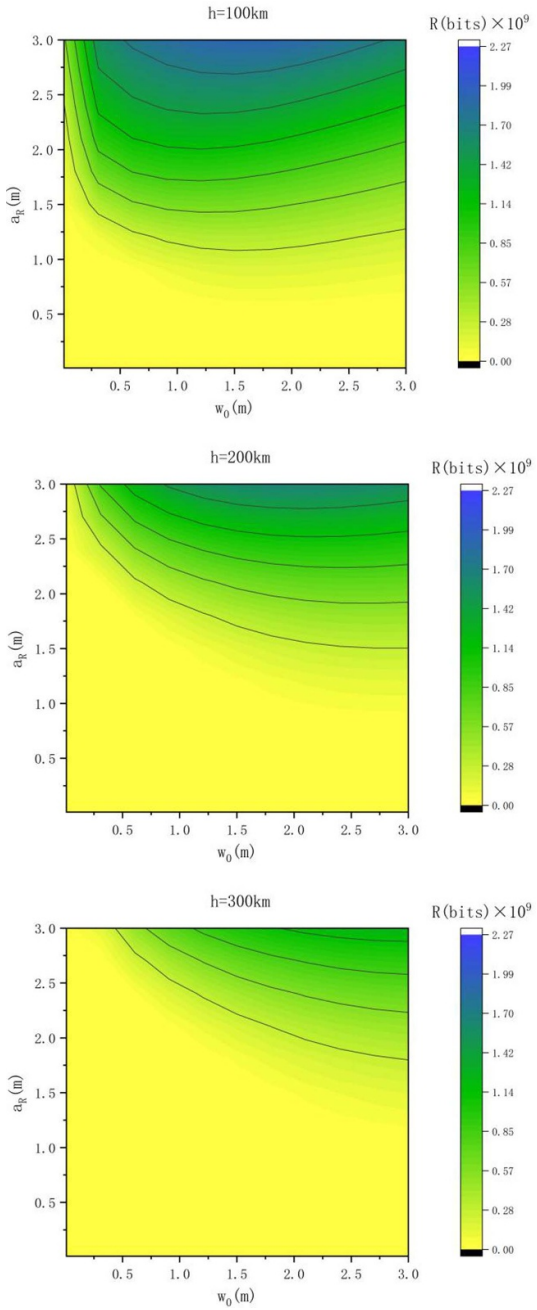

Figure 14. The influence of w_0 and a_R on the secure key, where $V = 2$ S.N.U. (a) $h = 100$ km. (b) $h = 200$ km. (c) $h = 300$ km.

the smaller the range of the modulation variance that can establish the non-zero secret key. For the altitude of 100 km, 200 km and 300 km, the optimal V can be set as 5.41, 2.61, 1.81 to obtain the maximized secure key.

After determining the selection of a_R, the combined effect of the modulation variance and the initial spot size on the secret key rate is shown in figure 17, and (a) (b) (c) are the contour maps of secure key at different altitude. The blue-green region is a non-zero secret key region. In figure 17(a), most regions can generate a secret key, and the dense contour line indicates that a small parameter change can have an obvious impact on the key rate. At the higher orbital altitude h shown in figure (b)(c), there are fewer optional combinations of V_A and w_0 that can generate key rates.

Figure 18 shows the secret key rate for different orbital altitudes. Where $a_R = 2.4$m, the initial spot size w_0 and the modulation variance V_A are set to be the optimal value according to the analysis of figure 17.

The orbit height affects the access time and transmission loss of the satellite. The visible communication time between satellite and the ground station is 135 s, 249 s and 318 s, respectively. According to Formula

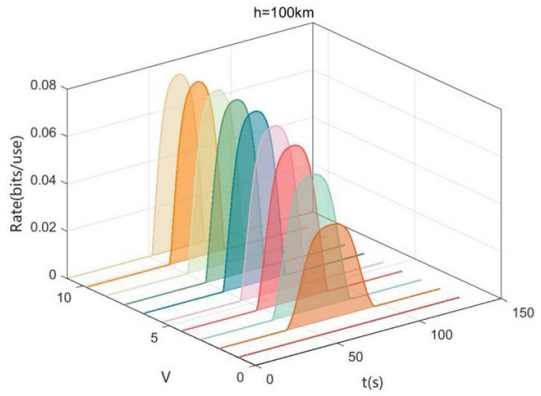

Figure 15. The real-time secret key rate under different V, where $h = 100$ km, $a_R = 2.4$ m, and $w_0 = 0.6$ m.

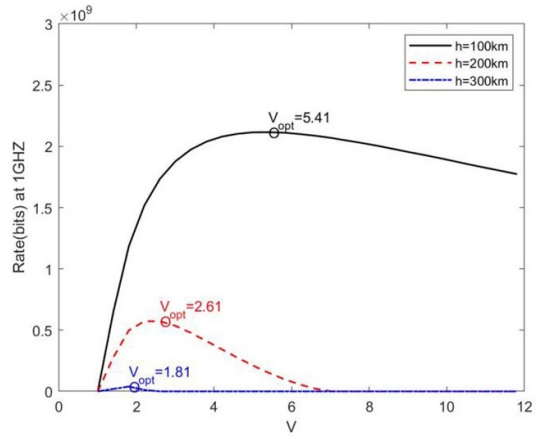

Figure 16. The secure key at different V, where $a_R = 2.4$ m, and $w_0 = 0.6$ m.

(25), it can be calculated that the secure key of these three satellite orbits during one transmission are 2.29×10^9bits, 1.29×10^8bits, and 8.23×10^8bits, respectively. In this study, the aperture of the receiving telescope is optimistically selected and some optimization parameters are carried out. Compared with the three satellite orbits, the lowest satellite obtains the maximum secure key.

4. Conclusion

In contrast to the traditional fixed circular orbit model, this study adopts a dynamic satellite orbit model for a practical discussion on the feasibility of uplink CV-QKD for VLEO satellites. The research encompasses the modeling of uplink scenarios involving ground station transmission and satellite reception, theoretical analysis of the spatially time-varying degradation channel, and estimation of the key generation rate for the CV-QKD protocol. The feasibility of CV-QKD with dynamic geometric parameter is performed under the uplink scene modeling, which can provide parameters selection and theoretical support for the future free space CV-QKD experiments.

This study also discusses the influence of modulation variance, initial spot size, and receiving telescope aperture on the secret key rate. 'We demonstrate that the aperture of the receiving telescope and the satellite orbit's altitude, both closely associated with atmospheric turbulence, significantly influence the secret key rate. The simulation outcomes provide optimal parameter selections that yield the highest secure key rates across a range of orbital heights. It is also important to recognize that the parameter selection like a_R may be overly optimistic. The primary rationale is the challenges encountered in uplink key distribution, notably the non-negligible impact of atmospheric turbulence, an effect that is mitigated in downlink scenarios. Nonetheless, from the analytical standpoint of parameter assessment, this study yields valuable insights and

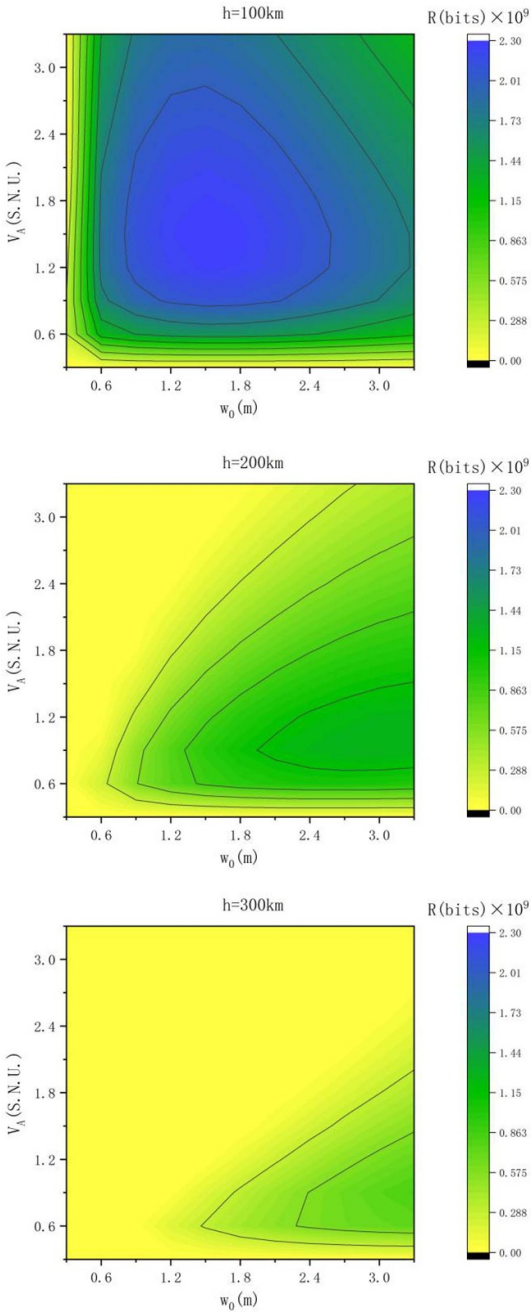

Figure 17. The influence of w_0 and V on the secret key, where $a_R = 2.4$ m. (a) $h = 100$ km. (b) $h = 200$ km. (c) $h = 300$ km.

lays a theoretical groundwork, offering guidance for the optimization of parameters in CV-QKD under more realistic conditions in future applications.

Furthermore, subsequent research will focus on harnessing intelligent optimization algorithms for channel compensation, which holds great promise in mitigating the effects of atmospheric turbulence, finite-length effects [23], and the Doppler effect [28]. This approach aims to identify the optimal parameter combinations, thereby enhancing the feasibility and practicality of uplink CV-QKD.

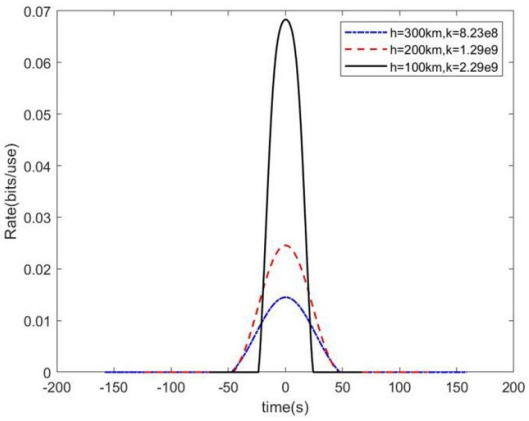

Figure 18. The secret key rate for different orbital altitudes where $a_R = 2.4$m, and w_0, V_A are optimized.

Data availability statement

All data that support the findings of this study are included within the article (and any supplementary files).

Acknowledgment

This work is supported by the National Natural Science Foundation of Hubei Province. (No.2024AFB991).

ORCID iDs

Ao Liu https://orcid.org/0009-0004-7852-7117
Wenbo Liu https://orcid.org/0000-0002-0089-8709
Chen Dong https://orcid.org/0000-0003-2745-0258

References

[1] Zhang Y, Bian Y, Li Z, Yu S and Guo H 2024 Continuous-variable quantum key distribution system: past, present, and future *Appl. Phys. Rev.* **11** 011318
[2] Lodewyck J, Bloch M, Garcia-Patron R, Fossier S, Karpov E, Diamanti E, Debuisschert T, Cerf N J, Tualle-Brouri R, McLaughlin S W and Grangier P 2007 Quantum key distribution over 25 km with an all-fiber continuous-variable system *Quantum Phys.* **2** 042305
[3] Liao K S *et al* 2017 Satellite-to-ground quantum key distribution *Nature* **549** 43
[4] Yehia R, Schiavon M, Acosta V M, Coopmans T, Kerenidis I, Elkouss D and Diamanti E 2023 Connecting quantum cities: simulation of a satellite-based quantum network **26** 073015
[5] Guo H, Li Z, Yu S and Zhang Y 2021 Toward practical quantum key distribution using telecom components *Fundam. Res.* **1** 96–98
[6] Dequal D, Trigo Vidarte L, Rodriguez V R, Vallone G, Villoresi P, Leverrier A and Diamanti E 2021 Feasibility of satellite-to-ground continuous-variable quantum key distribution *npj Quantum Inf.* **7** 1–10
[7] Pirandola S 2021 Limits and security of free-space quantum communications *Phys. Rev. Res.* **3** 013279
[8] Pirandola S 2021 Satellite quantum communications: fundamental bounds and practical security *Phys. Rev. Res.* **3** 023130
[9] Shengjie X, Yin L, Wang Y, Mao Y, Zuo Z, Ruan X and Guo Y 2021 Noiseless attenuation for continuous-variable quantum key distribution over ground-satellite uplink *Appl. Sci.* **11** 11289
[10] Hosseinidehaj N, Babar Z, Malaney R, Ng S X and Hanzo L 2019 Satellite-based continuous-variable quantum communications: state-of-the-art and a predictive outlook *IEEE Commun. Surv. Tutor.* **21** 881–919
[11] Wang X, Dong C, Zhao S, Yong L, Liu X and Zhu H 2021 Feasibility of space-based measurement-device-independent quantum key distribution *New J. Phys.* **23** 045001
[12] Marulanda Acosta V, Dequal D, Schiavon M, Montmerle-Bonnefois A, Lim C B, Conanm J-M and Diamanti E 2024 Analysis of satellite-to-ground quantum key distribution with adaptive optics *New J. Phys.* **26** 023039
[13] Lognoné P, Conan J-M, Paillier L, Védrenne N and Rekaya G 2022 Channel model of a ground to satellite optical link pre-compensated by adaptive optics *Signal Processing in Photonic Communications 2022*
[14] Montmerle Bonnefois A *et al* 2022 Feasibility demonstration of AO pre-compensation for GEO feeder links in a relevant environment *Opt. Express* **30** 47179–98
[15] Lognoné P, Conan J-M, Rekaya G and Védrenne N 2023 Phase estimation at the point-ahead angle for AO pre-compensated ground to GEO satellite telecoms *Opt. Express* **31** 3441–58
[16] Chai G 2020 *Investigation on Key Technologies of Free-space Continuous-variable Quantum Key Distribution* (Northwest University) (in Chinese)
[17] Wang S Y, Huang P, Wang T and Zeng G H 2018 Atmospheric effects on continuous-variable quantum key distribution *New J. Phys.* **20** 083037

[18] Andrews L C, Miller W B and Ricklin J C 1993 Geometrical representation of Gaussian beams propagating through complex paraxial optical systems *Appl. Opt.* **32** 5918–29
[19] Vasylyev D Y, Semenov A A and Vogel W 2012 Toward global quantum communication: beam wandering preserves nonclassicality *Phys. Rev. Lett.* **108** 220501
[20] Ruppert L, Peuntinger C, Heim B, Günthner K, Usenko V C, Elser D, Leuchs G, Filip R and Marquardt C 2019 Fading channel estimation for free-space continuous-variable secure quantum communication *New J. Phys.* **21** 123036
[21] Devetak I and Winter A 2003 Distillation of secret key and entanglement from quantum states *Quantum Phys.* **461** 207–35
[22] Fossier S, Diamanti E, Debuisschert T, Tualle-Brouri R and Grangier P 2009 Improvement of continuous-variable quantum key distribution systems by using optical preamplifiers *J. Phys.* B **42** 114014–23
[23] Anthony L, Frederic G and Philippe G 2010 Finite-size analysis of a continuous-variable quantum key distribution *Phys. Rev.* A **81** 062343
[24] Laudenbach F, Pacher C, Fred Fung C H, Poppe A, Peev M, Schrenk B, Hentschel M, Walther P and Hübel H 2018 Continuous-variable quantum key distribution with Gaussian modulation–the theory of practical implementations *Adv. Quantum Technol.* **1** 1800011
[25] Michael W *et al* 2023 The James Webb Space Telescope Mission: optical telescope element design, development, and performance *Publ. Astron. Soc. Pac.* **135** 058001
[26] Lillie C F 2005 Large deployable telescopes for future space observatories UV/Optical/IR Space Telescopes:Innovative Technologies and Concepts II
[27] Orsucci D, Kleinpaß P, Meister J, De Marco I, Häusler S, Strang T, Walenta N and Moll F 2024 Assessment of practical satellite quantum key distribution architectures for current and near-future missions (arXiv:2404.05668 [quant-ph])
[28] Ali I, Al-Dhahir N and Hershey J E 1998 Doppler characterization for LEO satellites *IEEE Trans. Commun.* **46** 309–13